THE UNIVERSITY OF MICHIGAN

College of Engineering

Department of Mechanical Engineering

Cavitation and Multiphase Flow Laboratory

Report No. UMICH 03371-9-T

NORMAL IMPACT OF A FINITE CYLINDRICAL LIQUID JET ON A FLAT RIGID PLANE

by

Yen C. Huang*
F. G. Hammitt**
Wen-Jei Yang***

(Submitted for Publication to Journal Fluid Mechanics)

Financial Support Provided by:

National Science Foundation
Grant No. GK-730

August 1971

* Research Associate (Formerly Doctoral Candidate)
** Professor-In-Charge, Cavitation and Multiphase Flow Laboratory
*** Professor

ABSTRACT

The normal impact of a flat-ended cylindrical water jet of finite length upon a rigid plane is studied. Particular emphasis is given the unsteady-state portion during the initial portion of the process. The governing partial differential equations of compressible flow, neglecting body force, viscosity and surface tension, are solved numerically by a newly developed Compressible-Cell-and-Marker (ComCAM) solution method. Numerical results are first checked by solving the classical one-dimensional "water hammer" problem (Huang, 1971).

Pressure build-up and lateral flow begin simultaneously with the impact, but the radial expansion of the cylindrical jet near the contact edge is not appreciable during this earliest stage of impact. A zone of negative pressure appears in the upper region of the finite cylindrical jet but there is no "bursting out" of the back surface. The maximum pressure in the finite cylindrical jet impact is found to be less than the one dimensional maximum pressure corrected for velocity of sound variation (85%)*. However, it is somewhat greater than the conventional "water hammer pressure" (uncorrected for density or velocity of sound variation).** The maximum lateral velocity, however, is greater than the impact velocity. As time elapses, the peak pressure on the impact surface shifts from the center radially outward, while the pressure at the center attenuates to the stagnation pressure.

---

*$\Delta p = \frac{\rho_o V_o C}{g_o}$

**$\Delta p = \frac{\rho_o V_o C_o}{g_o}$

NOMENCLATURE

Symbol	Description
A	Exponent in Tait's equation of state
B	Constant in Tait's equation of state
C	Shock wave velocity
C_o	Sonic Velocity
D	Diameter
H_1, H_2	Dimensions of Computation Domain in z- and r- direction, respecitvely
K	Constant
L	Length
M	Mach number
p	Pressure
p^o	$p/\rho_o C_o V_o$
R	Radius
R_m	Location of marker m in r- coordinate
r	Radial coordinate
r^o	r/R
t	Time
t^o	Non-dimensional time, Ct/D
U	Marker velocity component in z-direction
u	Velocity component in z-direction
u_n	Velocity component in normal direction
V	Marker velocity component in r-direction
v	Velocity component in r-direction
v_t	Velocity component in tangential direction
V_o	Impact velocity
x_n	Coordinate in normal direction
x_t	Coordinate in tangential direction
z	Vertical coordinate

z^o	z/L
Z_m	Location of marker m in z-coordinate
α	Stability factor
ρ	Density
Δ	Increment

Subscripts

c	Characteristic parameter
m	Marker index
n	Normal direction
o	Initial value
t	Tangential direction

Superscripts

o	Non-dimensional variable

LIST OF FIGURE CAPTIONS

Figure	Caption
1	Shape-time history of an initially cylindrical droplet with L/D = 1, at impact Mach number of 0.2 and under free-slip boundary condition.
2a-e	Isobar distribution in an initially cylindrical droplet with L/D = 1 at time Ct/D = 0.125, 0.25, 0.5, 1.0, 2.5 for impact Mach number of 0.2 and under free-slip boundary condition.
3	Pressure-time history at liquid-solid interface (z=0) of an initially cylindrical droplet with L/D = 1, for impact Mach number of 0.2 and under free-slip boundary condition.
4	Pressure-time history along the symmetrical axis (r=0) of an initially cylindrical droplet with L/D = 1 for impact Mach number of 0.2 and under free-slip boundary condition.
5	Local pressure-time history at a(r=0, z=0.5 L), b(r=0, z=0) and c(r=0.75R, z=0) in an initially cylindrical droplet with L/D =1 for impact Mach number of 0.2 and under free-slip boundary condition.
6	Radial velocity-time history at liquid-solid interface (r=0) of an initially cylindrical droplet with L/D = 1, for impact Mach number of 0.2 and under free-slip boundary condition.
7	Maximum pressure gradient-time and-location relation and contact edge-time history of an initially cylindrical droplet with L/D=1, for impact Mach number of 0.2 and under free-slip boundary condition.

I. INTRODUCTION

When a cylindrical free jet of water is directed perpendicularly against a rigid smooth wall, the jet is deflected into lateral flow parallel to the wall away from the point of impact. Most previous studies of this problem deal with the steady state. Bernoulli's theorem is often used to simplify the analysis for regions away from the stagnation point. Approximately uniform lateral velocity and pressure are predicted. Thickness of lateral flow is all that remains to be determined (Batchelor, 1967). For the region near the stagnation point, the velocity distribution conventionally is assumed, and then pressure is calculated by potential flow theory (Schlichting, 1960).

However, at the first instant of impact, the sudden change of boundary velocity will establish large pressure gradients, which in turn produce a sudden change in the velocity at every point of the fluid. The velocities and their spatial gradients are negligible compared to the local acceleration in this impulsive motion. Problems involving a sudden change of velocity at a portion of the boundary, similar to the present case, arise in connection with the impact of a liquid jet on the solid surface of a target or a projectile on the free surface of a stationary body of liquid. A severe local pressure of the order of 5000atm. is predicted over a very short duration of 0.25×10^{-6} sec. for an impact velocity of 1000 ft/sec.

The main objective of the present study was to investigate analytically the unsteady features of liquid-solid impact by formulating the transient, two-dimensional governing equations plus the equation of state for water. Then, using numerical techniques, the flow patterns and impact pressure and velocity distribution developed in a cylindrical jet of water following its collision with a plane rigid surface, would be found.

II. ANALYSIS

When a free cylindrical jet of water impinges on a rigid surface, the water is diverted into lateral flow. Equations and boundary conditions describing the situation are well-known, but it is a formidable and probably impossible task to obtain a closed form solution. However, a numerical approach wherein one treats the liquid as a distributed system, subjected to the boundary condition at the interface with solid and gas, is possible.

The compressibility of the liquid must be taken into account in any valid and realistic analysis, since otherwise an unrealistic infinitely large pressure will be produced at the first instant of impact. Unless the impact velocity is extremely small, compressibility effects predominate in the liquid response during the period of unsteadiness. However, it is reasonable to neglect the effect of body force and viscosity as can be easily shown by comparing with impact pressure magnitude. Surface tension which effects the boundary condition can also be neglected. Cylindrical coordinates are natural for the problem. Then the governing equations for a cylindrical liquid jet colliding with a rigid solid surface are as follows.

Continuity and momentum for the liquid gives:

$$\frac{\partial \rho}{\partial t} + \frac{\partial(\rho u)}{\partial z} + \frac{1}{r}\frac{\partial(r\rho v)}{\partial r} = 0 \tag{1}$$

$$\frac{\partial(\rho u)}{\partial t} + \frac{\partial(\rho u^2)}{\partial z} + \frac{1}{r}\frac{\partial(r\rho vu)}{\partial r} = -\frac{\partial p}{\partial z} \tag{2}$$

$$\frac{\partial(\rho v)}{\partial t} + \frac{\partial(\rho uv)}{\partial z} + \frac{1}{r}\frac{\partial(r\rho v^2)}{\partial r} = -\frac{\partial p}{\partial r} \tag{3}$$

and Tait's equation of state for water (Tait, 1888) is:

$$\frac{p + B}{p_o + B} = \left(\frac{\rho}{\rho_o}\right)^A \tag{4}$$

u and v are the axial and radial velocity components respectively for the cylindrical coordinates z and r. Time t is another independent variable, and

and p are the fluid density and pressure. The values of A and B in Tait's equation of state for water are chosen as (Cole, 1965):

A = 7.15 and B = 3.047 kilobars.

The above set of (1) through (4), which are in the Eulerian form, are used to find impact pressure and velocity distribution within the liquid

The following set of equations for marker particles, which are in Lagrangian form, are required to indicate the movement and location of the liquid boundary.

$$\frac{d(\rho U)}{dt} \cong -\frac{dp}{dz} \tag{5}$$

$$\frac{d(\rho V)}{dt} \cong -\frac{dp}{dr} \tag{6}$$

$$Z_m = \int U dt \tag{7}$$

$$R_m = \int V dt \tag{8}$$

Here, U and V are the marker velocity components in the z- and r- direction, while Z_m and R_m denote the coordinates in these directions.

The appropriate initial conditions over the domain of calculation are

$$p = p_o \qquad u = u_o \qquad v = v_o$$

where p_o is the ambient pressure, and u_o and v_o are the initial impact velocities in the z- and r- direction respectively. In the case of a normal impact (i.e., perpendicular), $v_o = 0$ of course and $V_o = u_o$, where V_o is the impact velocity.

The appropriate boundary conditions are:

i) along the axis of symmetry (z), r = 0, and symmetry requires

$$v = 0, \quad \frac{\partial u}{\partial r} = 0, \quad \frac{\partial p}{\partial r} = 0$$

ii) along the impacted rigid surface , z = 0, $\frac{\partial v}{\partial z} = 0$, u = 0, $\frac{\partial p}{\partial z} = 0$, for full-slip wall condition, which, strictly speaking an assumption of zero viscosity would necessitate; and v = 0, u = 0, $\frac{\partial p}{\partial z} = 0$ for a non-slip wall condition.

iii) along the free surface, the incompressible continuity condition yields

$$p = p_o, \quad \frac{\partial u_n}{\partial x_n} = \frac{\partial v_t}{\partial x_t} = 0$$

where u_n and v_t are the moving velocity components of the liquid-air interface in the normal x_n and tangential x_t directions of the surface respectively.

iv) along the sides of the finite computational domain, permeable boundary conditions will be imposed, in such a way that the normal space derivative of the variable vanishes at the boundary,

$$\frac{\partial u}{\partial z} = 0, \quad \frac{\partial v}{\partial z} = 0, \quad \frac{\partial p}{\partial z} = 0 \text{ at } z = H_1$$

$$\frac{\partial u}{\partial r} = 0, \quad \frac{\partial v}{\partial r} = 0, \quad \frac{\partial p}{\partial r} = 0 \text{ at } r = H_2$$

where H_1 and H_2 are the dimensions of the computational domain in the z- and r- direction, respectively.

All the above equations are then nondimensionalized and expressed in finite difference forms. A compressible-cell-and-marker numerical solution method was developed (Huang, 1971). The numerical computation starts with marker particles located along the interface to keep track of the deformation of the liquid boundary. Then pressure and velocity within the liquid boundary are calculated. The detailed descriptions of the method are given by the first author of the present paper, Huang (1971).

The numerical results represent approximate solutions to the original differential equations, since derivatives are replaced by finite differences. Terms of the order of the square of the time increment and spatial step size are neglected. The convergence of the finite difference representation, i.e., the degree to which the approximate solution approaches the exact solution, must then be examined.

It is known that although the explicit formulation avoids the need of iterative or matrix inversion techniques, the Courant stability criterion (Richtanyer & Morton, 1967), must be satisfied, i.e., the distance a wave travels in the time increment Δt must be less than the spatial step size Δz or Δr. That is:

$$\Delta t < \frac{\min.(\Delta z,\ \Delta r)}{C} \tag{9}$$

where C is the shock wave velocity in the liquid phase. With the definition of the stability factor

$$\alpha = \frac{C\ \Delta t}{\min.(\Delta z,\ \Delta r)} \tag{10}$$

one can satisfy the stability criterion by selecting a value of α less than unity.

Numerical experiments were carried out to determine the stability factor and required numbers of cells so that convergence of the result was reasonably assured, in regard to magnitudes, timing, and wave shapes. For the acutal study, a stability factor $\alpha = 0.1$ and 20 x 40 mesh were used.

III RESULTS AND DISCUSSION

In examining the results, one must consider the following. Constant atmospheric pressure at the water-air free surface is imposed. The impact plane, which is perfectly rigid and smooth, has no movement The water is assumed inviscid, without surface tension, but compressible and elastic. The fracture strength of water is taken to be 270 atm. an experimental result of Briggs (1950). Of course, ordinarily pure water will rupture at much smaller tensions, but perhaps not for the very short duration of tension involved here. The initial length of the cylindrical droplet is L and its diameter, D. The impact Mach number M is defined as V_o/C_o, where C_o is the sonic velocity in the undisturbed liquid.

Figure 1 shows how the shape of a droplet with L/D = 1 deforms as a function of time. The top of the droplet retains its original flat shape up to the non-dimensional time $t^o = Ct/D = 1$ (about equivalent to 1 μ sec for an impact Mach number of 0.2 with a 2 mm dia. droplet) after which it becomes convex. The liquid flows out radially parallel to the surface without apparently contacting it.

Figures 2a through 2e depict the isobar distribution in the droplet at various instants, i.e., t^o = 0.125, 0.25, 0.5, 1.0 and 2.5, respectively. The figures illustrate how the pressure waves propagate with time from the impacted surface toward the air-water free surface. Due to constant atmospheric pressure at this free surface, all the isobaric surfaces at small times appear as an inverted cup resting upon the impacted surface (Figure 2a). As time progresses and the droplet shrinks in height accompanied by radial-expansion (Figure 2b) each cup-shaped isobaric surface grows in size, both depth and width. The isobaric surfaces for

small values of $p^o = p/\rho_o C_o V_o$ still retain the inverted cup shape in the outer region of the droplet, for $t^o = 0.5$ (Figure 2c), those for medium pressure (in the inner portion) form egg-shape surfaces, coaxially arranged, with the smaller end pointing toward the impacted surface. In the central region of the droplet, however, the isobaric surfaces for large isobars appear as round-edged discs which are arranged concentrically with the major axes parallel to the impacted surface. The pressure patterns in the droplet result primarily from the effect of the rarefaction waves from the air-water free surface at the impacted edge. The pressure at the stagnation point ($r = 0$, $z = 0$) is released from the contact edge of the solid liquid interface rather than from the top of the droplet. The mechanism can be explained by the following approximate arguments.

Assume that the compression wave travels along the symmetrical axis at the approximate shock wave speed of C (Heymann, 1968).

$$C = C_o + KV_o \tag{11}$$

where K is some constant (about 2 for water). Further assume the rarefaction wave velocity is C_o. The minimum possible diameter, D_{min} of a cylindrical droplet of length L if the wavepattern near the axis of symmetry is to remain one-dimensional until a refraction wave has returned from the back of the drop is

$$D_{min} = 2\ L\ (\frac{2 + KM}{1 + KM}) \tag{12}$$

and

$$D_{min} = 4\ L, \text{if } M \ll 1 \tag{13}$$

Equation (13) indicates that rarefaction waves reach the stagnation point from the top of the drop before those from the periphery of the drop only when $L/D < 1/4$; i.e., when the droplet shape is actually a disc.

Figure 2d for $t^o = 1.0$ indicates the possibility of cavitation in that there is a region of negative pressure enclosed by the zero isobaric surface as a result of the rarefaction waves. However, no "bursting out" of the top surface appears. The isobaric surface of $p^o = 0.05$ froms a half doughnut shape which includes the region of high compressive pressure.

In Figure 2e ($t^o = 2.5$) the droplet shape has become that of a military helmet. The isobaric surfaces along the axis changes from convex to concave as p^o increases. The highest p^o values are confined to the half doughnut shape region over the solid surface near $r^o (= r/R) = 1.0$.

Better illustrations of the pressure distribution on the impacted surface and along the axis of symmetry are given in Figures 3 and 4, respectively. Figure 3 shows that the pressures build up immediately rather uniformly over the entire impacted surface except near the outer edge, where the boundary condition of atmospheric pressure has been satisfied. Figure 4 depicts how the pressure waves propagate along the axis of symmetry, starting from the impacted surface. These waves reach the top of the droplet at about $t^o = 0.5$ and then rebound, producing large regions of negative pressure. The pressure at the stagnation point (0, 0) is positive (compressive) until the rarefaction waves reach that point along the axis of symmetry ($r = 0$) or along the impact surface ($z = 0$). Its magnitude increases continuously (until the time t^o of about 0.25) at a much greater rate than the pressures over the rest of the impacted surface. At the same time, the rarefaction wave starts to affect the

pressure near the outer edge (Figures 3 and 4). The pressure at the stagnation point then decreases and actually becomes negative at time about 1.25 (Figure 5). It then rebounds and oscillates about the normalized steady-state stagnation pressure, which is $\frac{\rho_o V_o^2}{2} / \rho_o C_o V_o = \frac{M}{2} = 0.1$ for $M = 0.2$. The numerical computation was terminated at $t^o = 2.5$, since the steady state has been reasonably approached, and most of the important features of the liquid-solid impact have already been disclosed. Figure 5 also shows the pressure-time history at two other locations (0, 0.5) and (0.75, 0). The tension at point "a" (0, 0.5) has exceeded the assumed rupture pressure during the time t^o between 1 and 1.5, indicating the probability of cavitation at this location. However, such a cavity would be short-lived, since it will be subject to compression after $t^o = 1.5$. Since the pressure gradient on the impacted surface is the greatest near the contact edge as shown in Figure 3, the instantaneous radial velocity increment at the location must be correspondingly the largest (Figure 6).

Figure 6 shows the radial velocity distribution on the impacted surface. The dotted portion of the curves indicate regions where the jetting liquid does not remain in contact with the surface. The radial jetting velocity exceeds the impact velocity at $t^o = 0.2$.

The positive pressure gradient in the radial direction results in a positive time-rate of change in the radial velocity. Therefore as pressure gradients on the impacted surface change from positive to negative (Figure 3), the radial velocities on the impacted surface change correspondingly from increasing to decreasing (Figure 6). The maximum pressure gradient and its corresponding location on the impacted surface are given in Figure 7. The radial pressure gradient reaches its peak at $t^o = 0.2$ just inside the initial outer edge. It then decreases to its steady-state value as the location of the maximum pressure gradient moves outward.

IV. CONCLUSIONS

The object of this paper was to investigate the unsteady (very initial) features of liquid-solid impact. Effort was directed to study the effect of two-dimensionality with axisymmetry by selecting a flat-ended cylindrical jet of relatively small length. Pressure and velocity distributions were solved as a function of time. The following conclusions can then be drawn.

1. The unsteady period is relatively very short, but is the most important period during the liquid-solid impact from the viewpoint of surface damage.

2. Compressibility is the predominant effect in this period of liquid-solid impact.

3. Since the liquid surface is free to deform, the impacting jet is diverted into lateral (radial) flow immediately after impact. The pressure build-up is thereby affected from the first instant of contact.

4. The smaller is the length-diameter ratio L/D, the closer is the impact pressure to the one-dimensional maximum pressure (water hammer pressure with corrected sonic velocity) over a reasonable time interval. This approximation is reasonably valid if the minimum diameter is at least four times the cylinder length. The maximum pressure is then ~1.2 x the convention water hammer pressure*.

ACKNOWLEDGEMENT

The work was supported by National Science Foundation Grant No. GK 730

---

* $\Delta p = \dfrac{\rho_o C_o V_o}{g_o}$

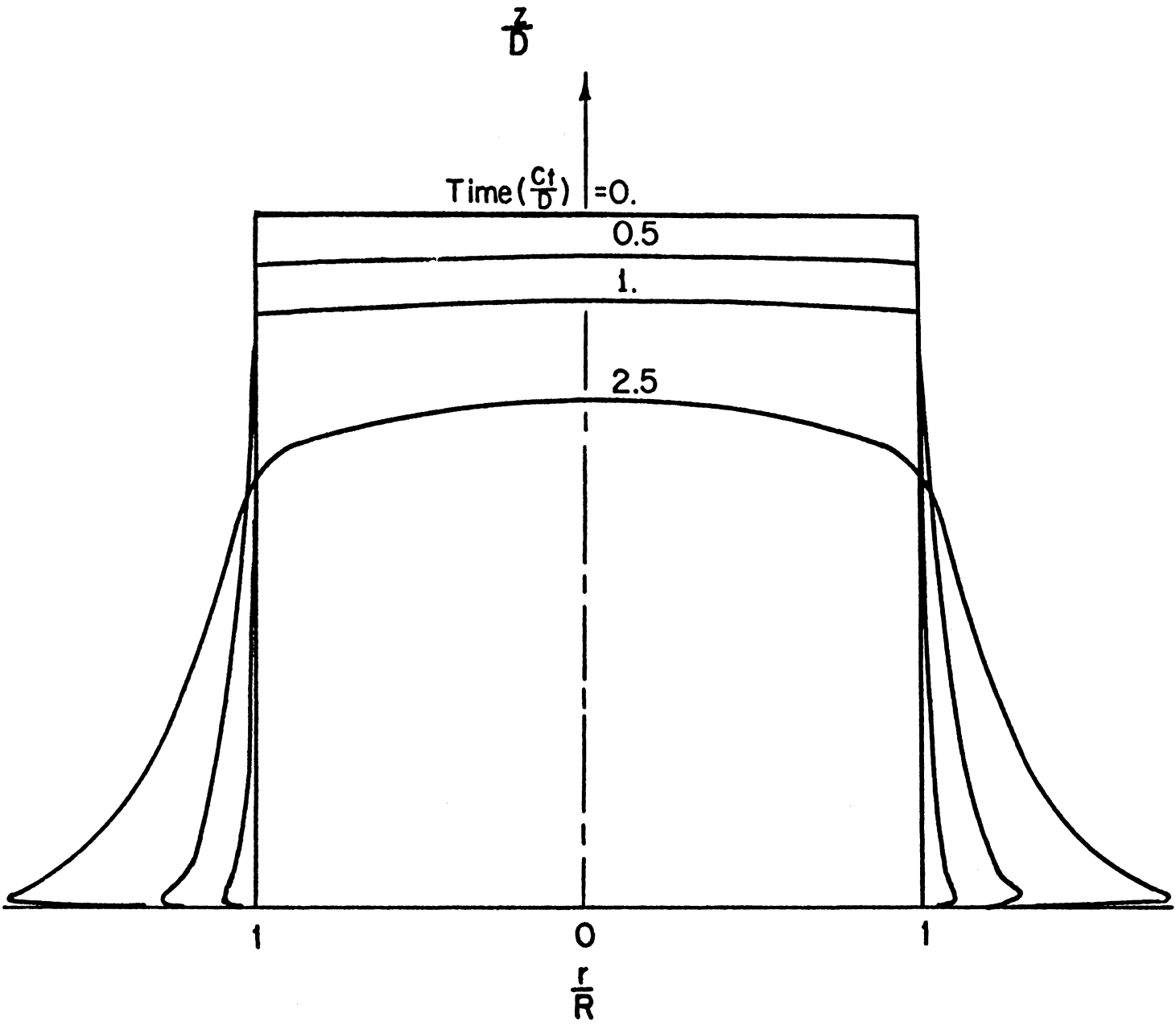

Fig. 1. Shape-Time History of an Initially Cylindrical Droplet with L/D = 1, at Mach Number = 0.2, for Free-Slip Boundary Condition.

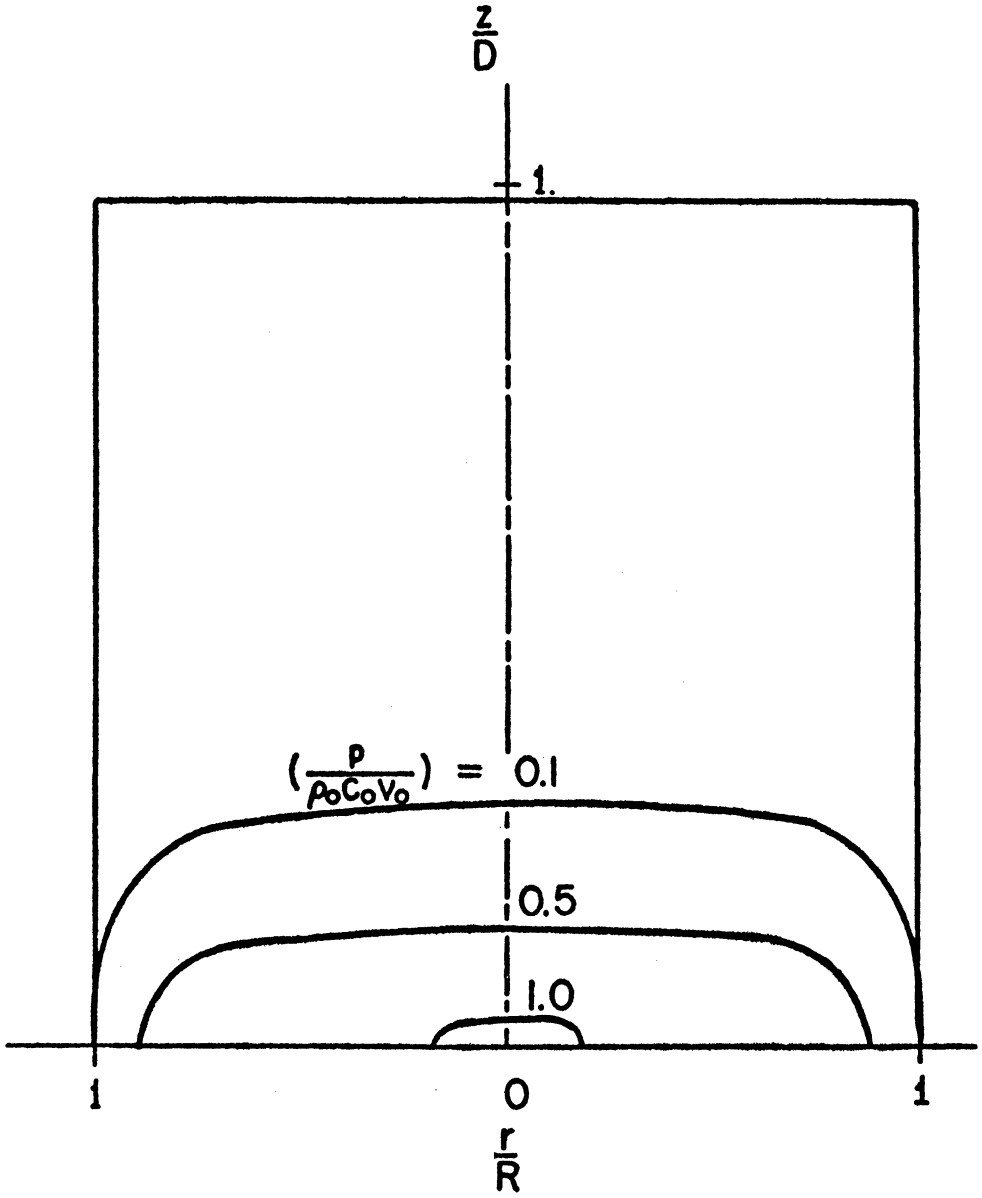

Fig. 2a. Isobar Distribution in an Initially Cylindrical Droplet with L/D = 1, at Time (Ct/D) = 0.125, for Impact Mach Number of 0.2 and for Free-Slip Boundary Condition.

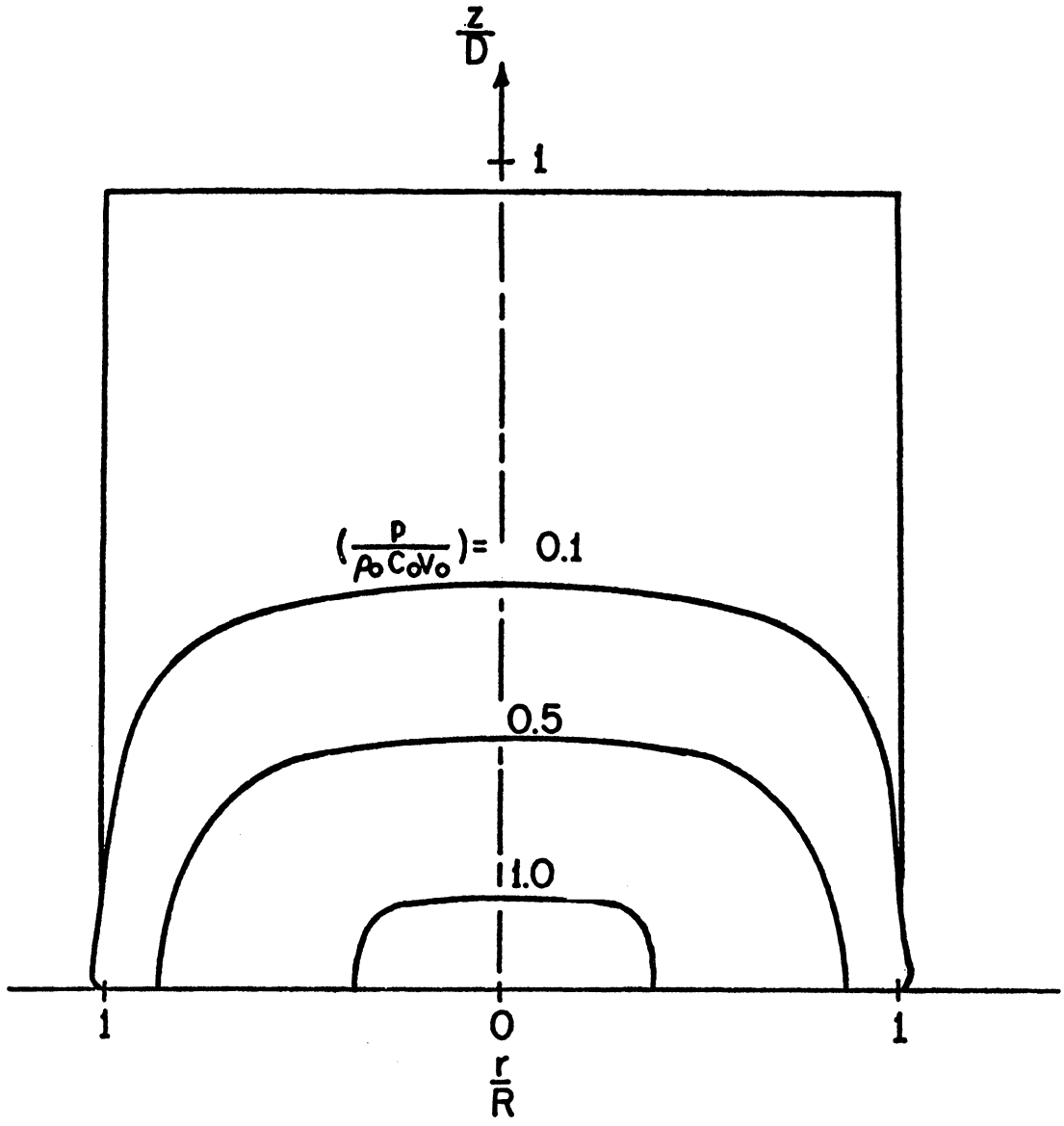

Fig. 2b. Isobar Distribution in an Initially Cylindrical Droplet with L/D = 1, at Time (Ct/D) = 0.25, for Impact Mach Number of 0.2 and for Free-Slip Boundary Condition.

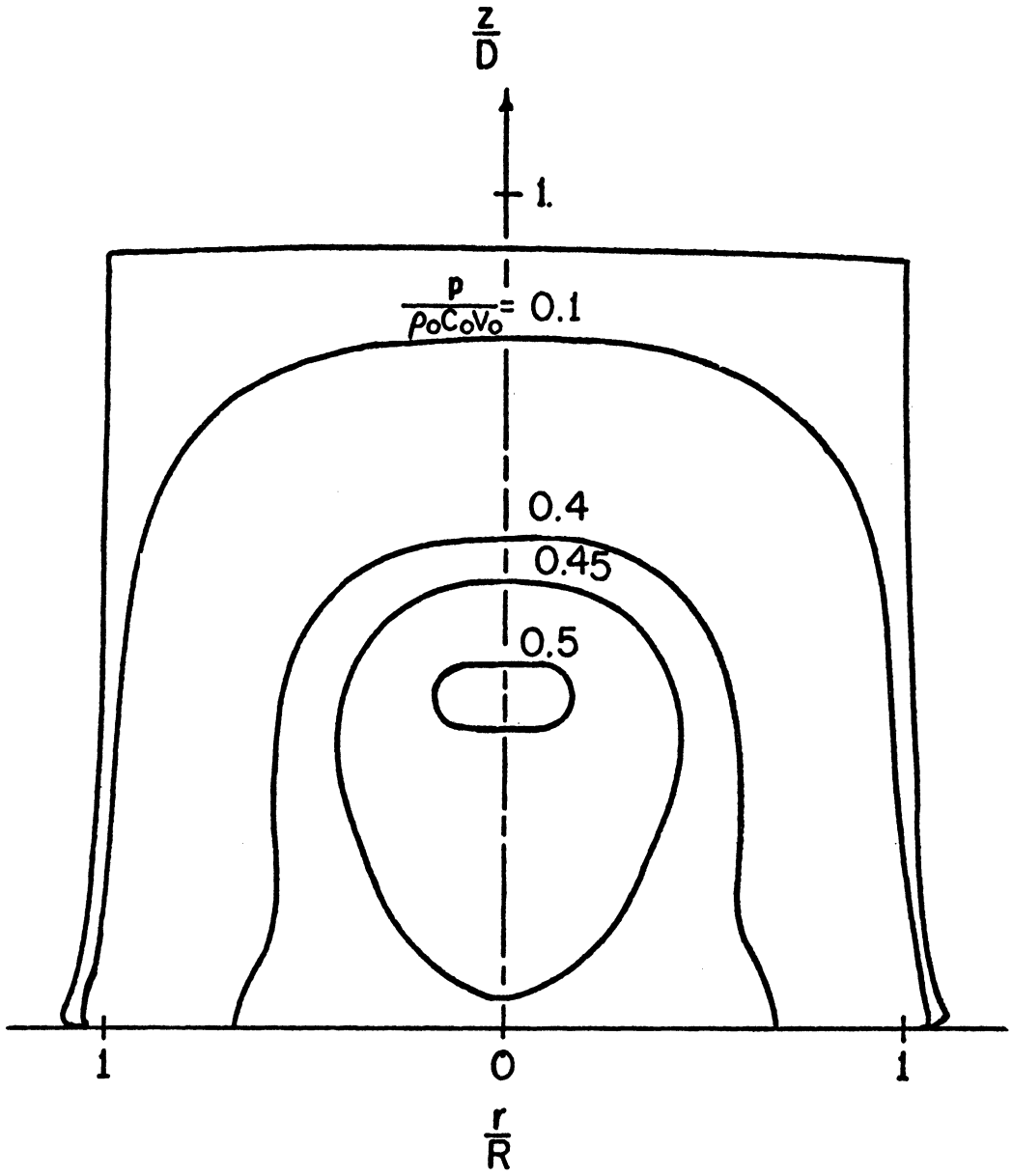

Fig. 2c. Isobar Distribution in an Initially Cylindrical Droplet with L/D = 1, at Time (Ct/D) = 0.5, for Impact Mach Number of 0.2 and for Free-Slip Boundary Condition.

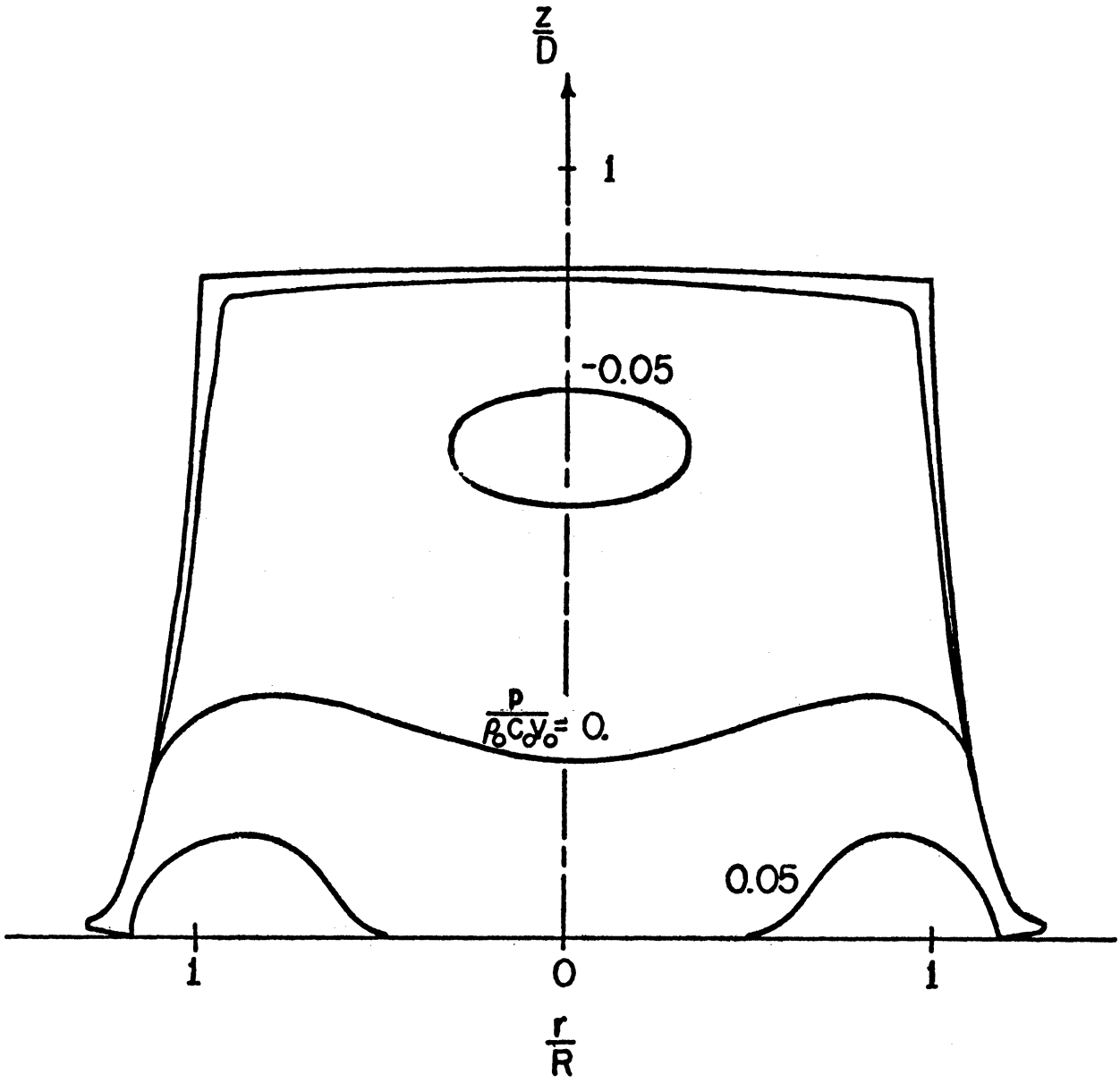

Fig. 2d. Isobar Distribution in an Initially Cylindrical Droplet with L/D = 1, at Time (Ct/D) = 1, for Impact Mach Number of 0.2 and for Free-Slip Boundary Condition.

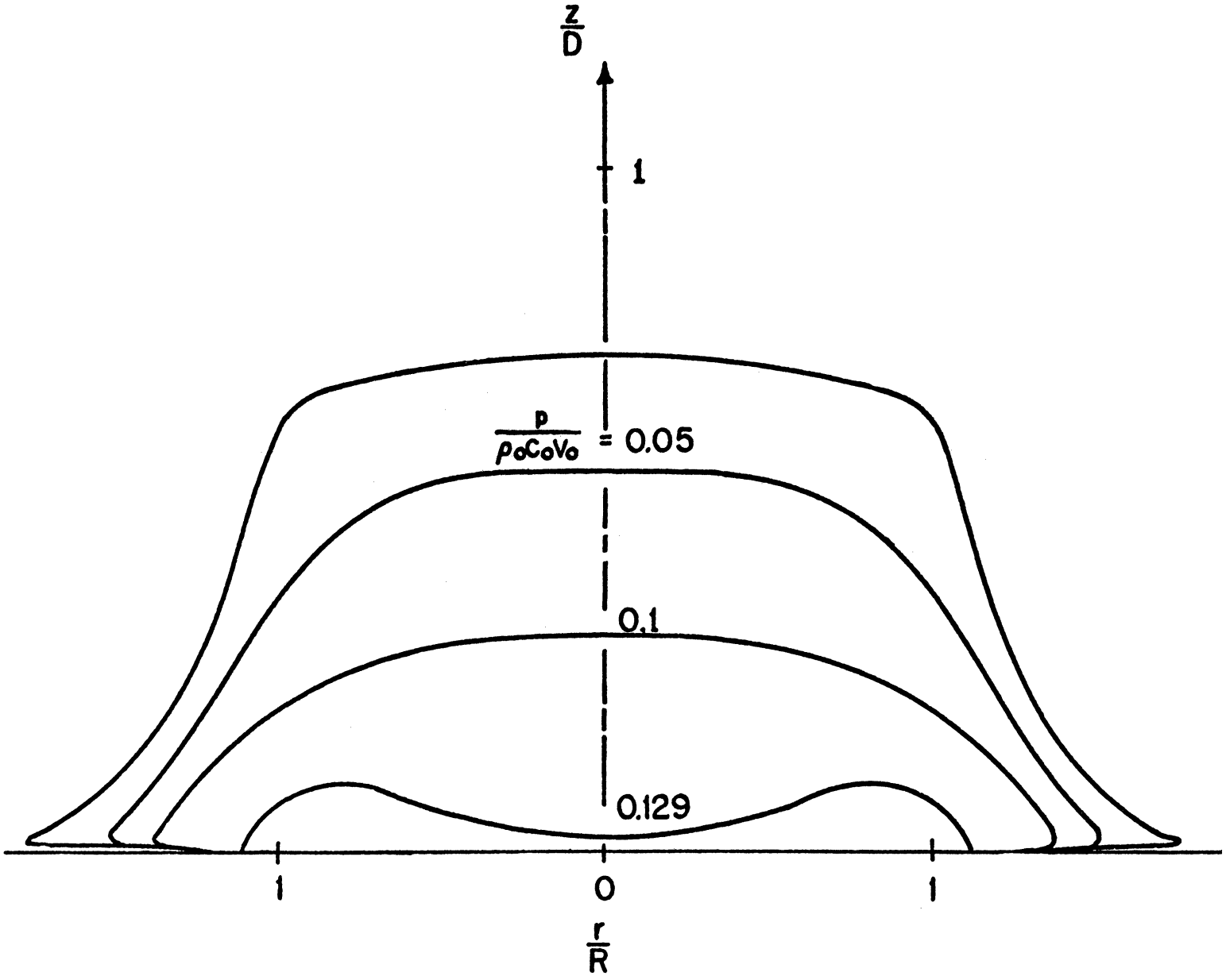

Fig. 2e. Isobar Distribution in an Initially Cylindrical Droplet with L/D = 1, at Time (Ct/D) = 2.5, for Impact Mach Number of 0.2 and for Free-Slip Boundary Condition.

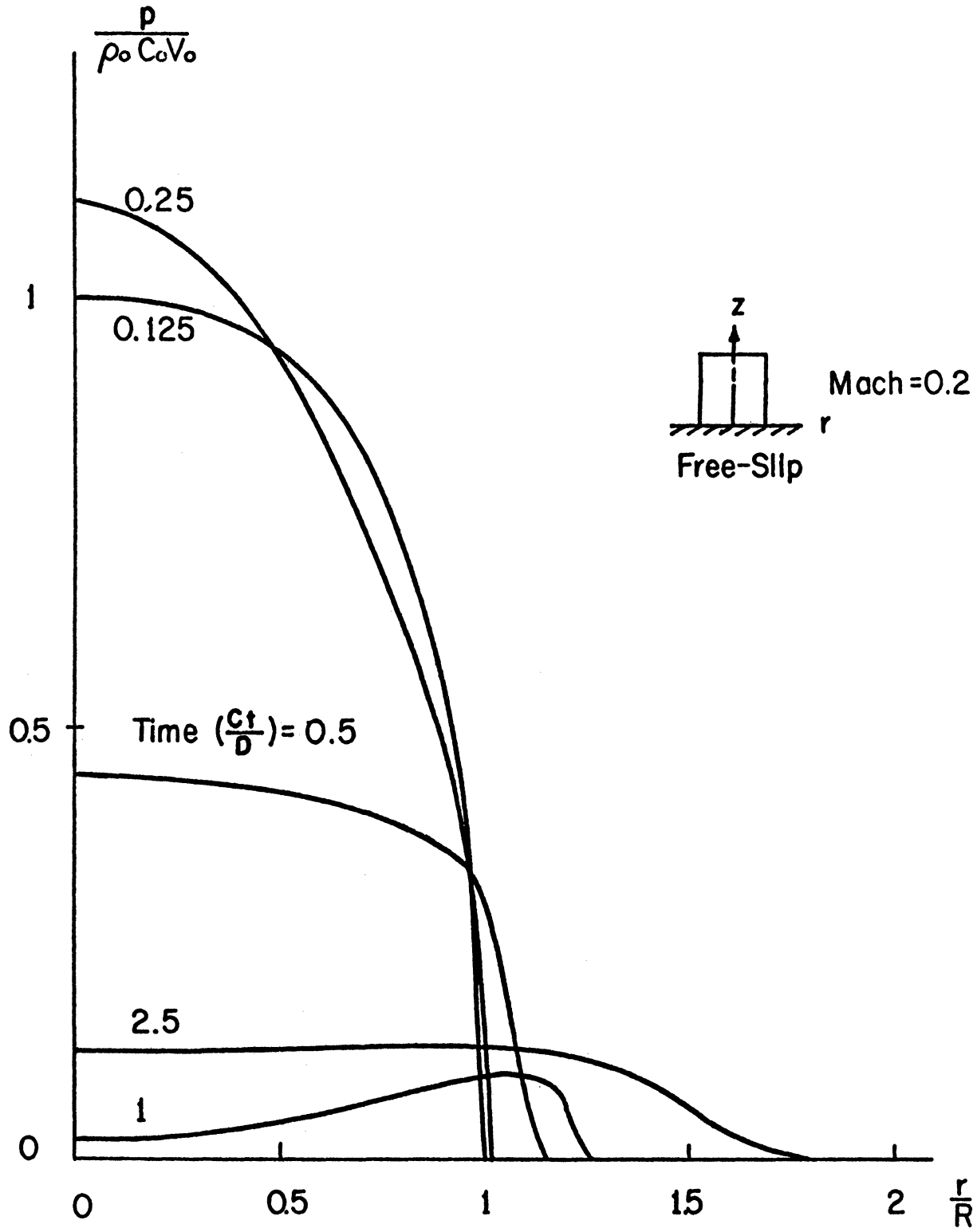

Fig. 3. Pressure-Time History at Liquid-Solid Interface (z = 0) of an Initially Cylindrical Droplet with L/D = 1, for Impact Mach Number of 0.2 and for Free-Slip Boundary Condition.

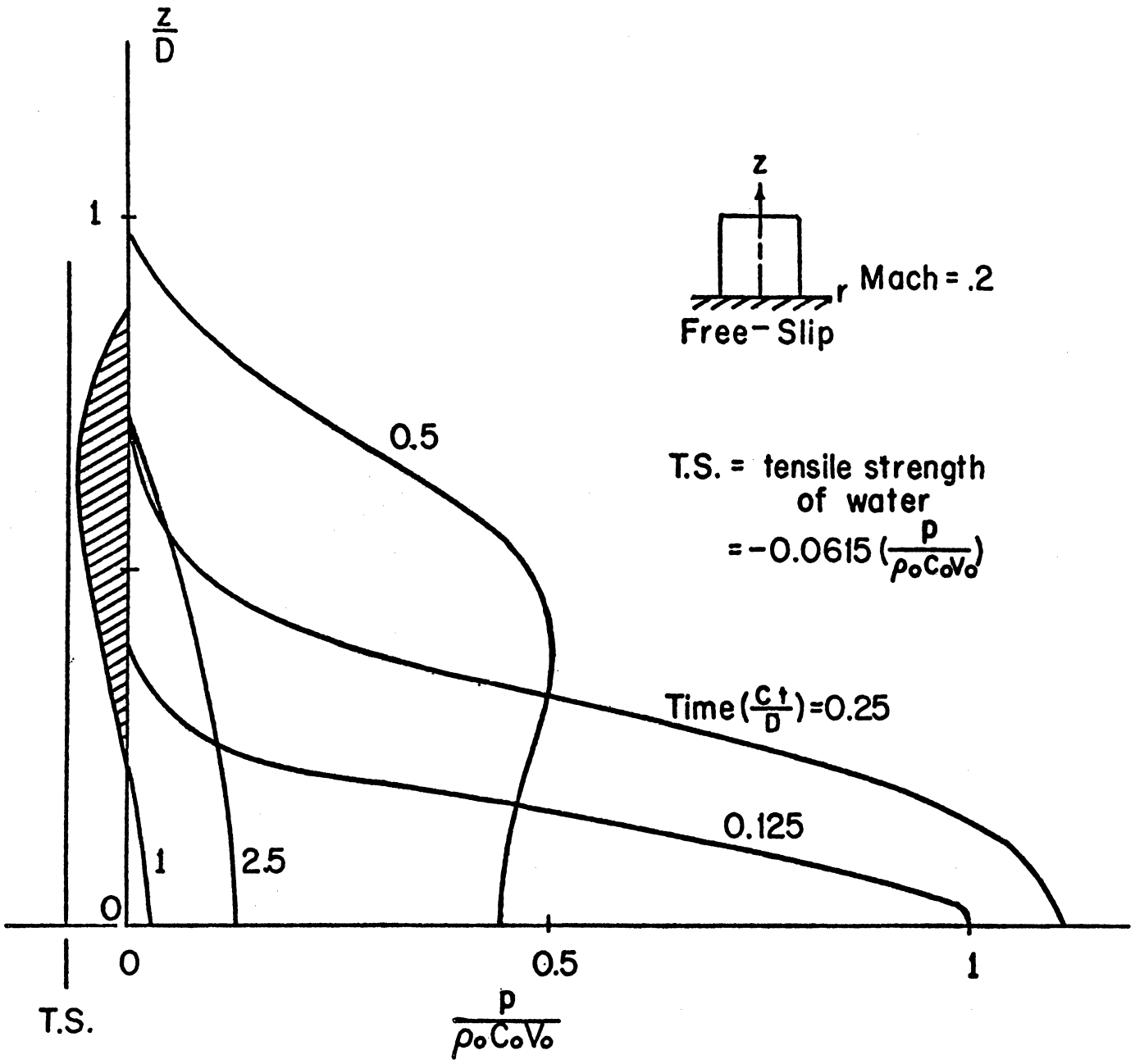

Fig. 4. Pressure-Time History along the Symmetrical Axis (r = 0) of an Initially Cylindrical Droplet with L/D = 1, for Impact Mach Number of 0.2 and for Free-Slip Boundary Condition.

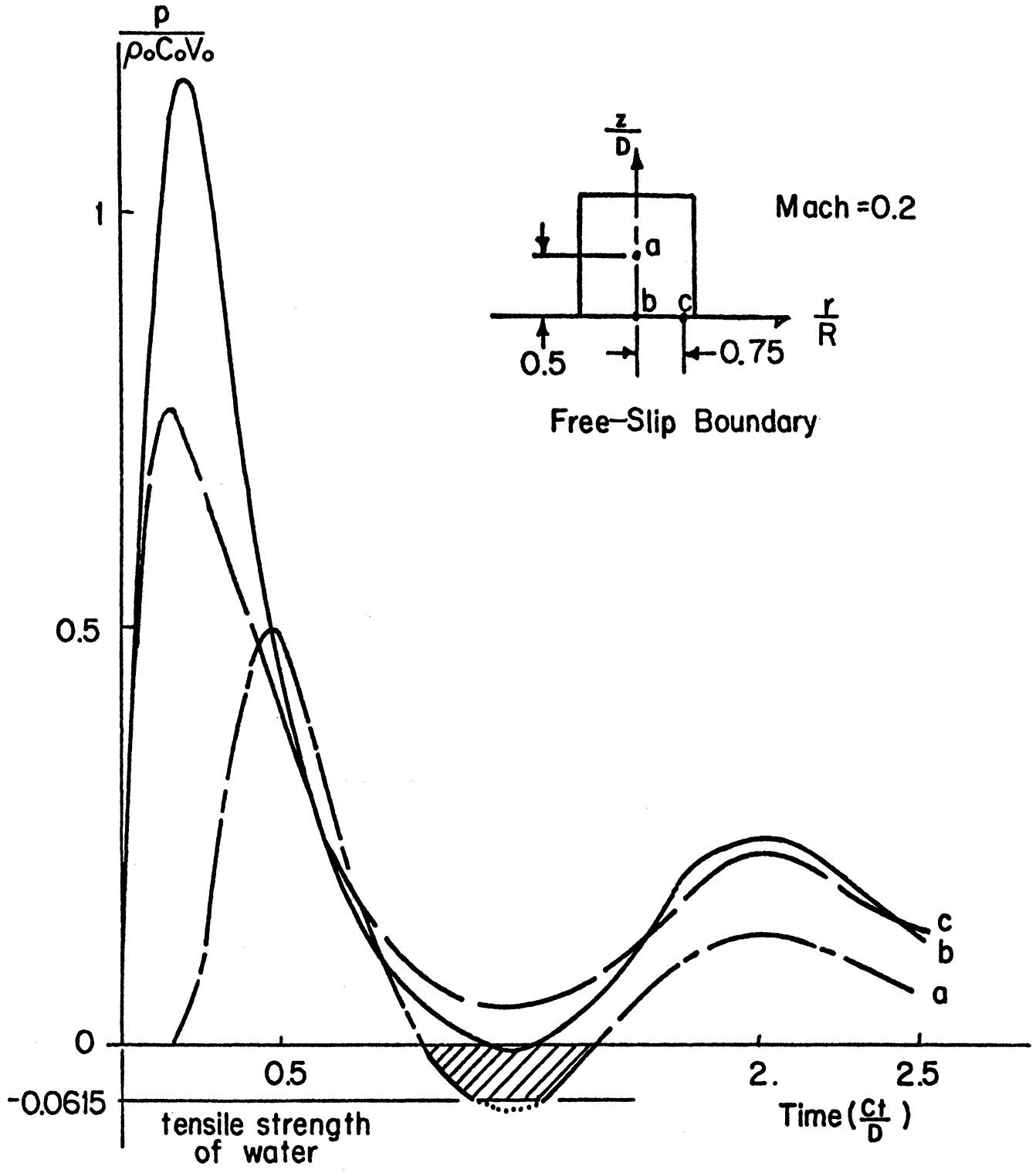

Fig. 5. Local Pressure-Time History at a (r = 0, z = 0.5L), b (r = 0, z = 0), and c (r = 0.75R, z = 0), in an Initially Cylindrical Droplet with L/D = 1, for Impact Mach Number of 0.2 and for Free-Slip Boundary Condition.

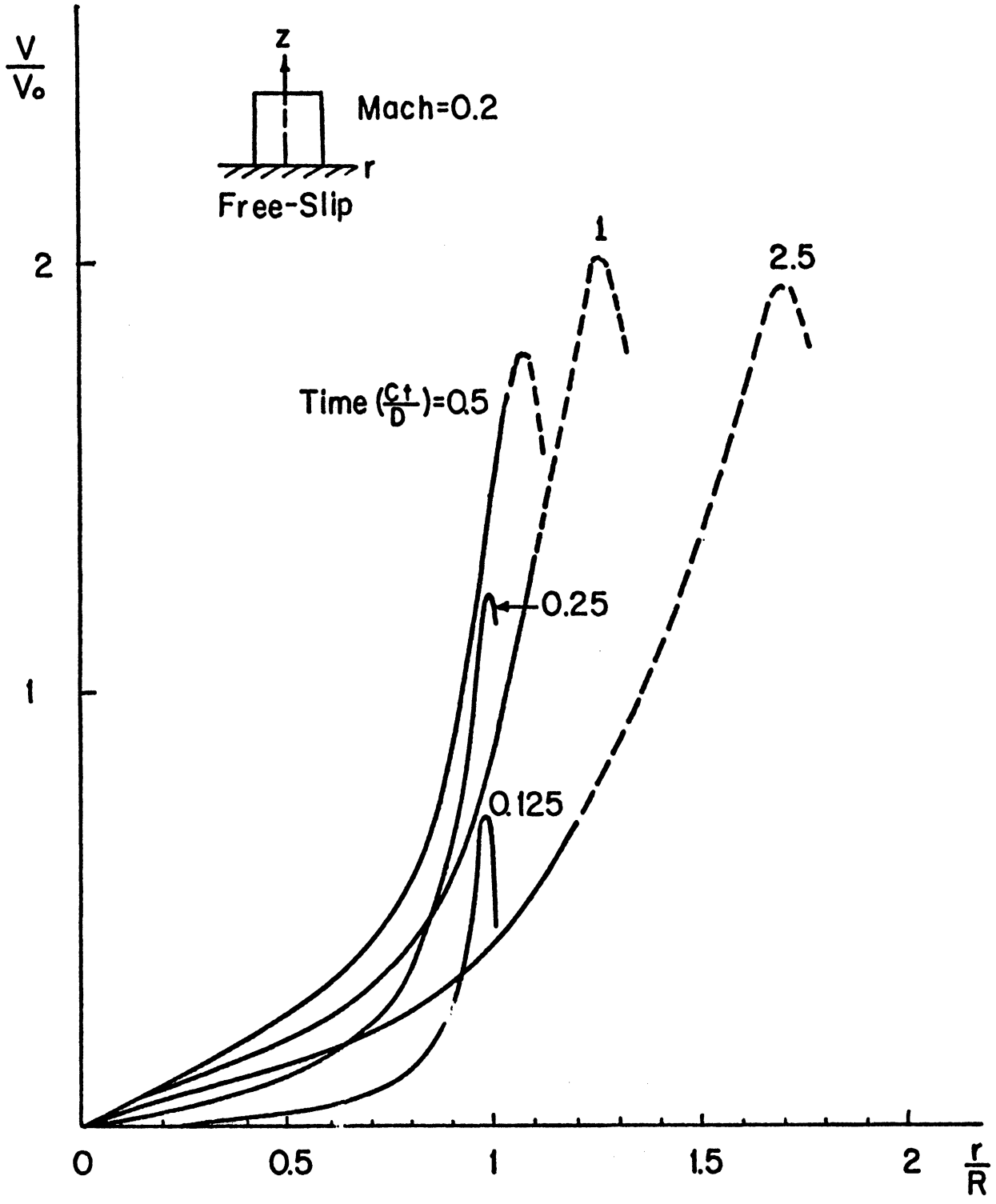

Fig. 6. Radial Velocity-Time History at Liquid-Solid Interface (r = 0) of an Initially Cylindrical Droplet with L/D = 1, for Impact Mach Number of 0.2 and for Free-Slip Boundary Condition.

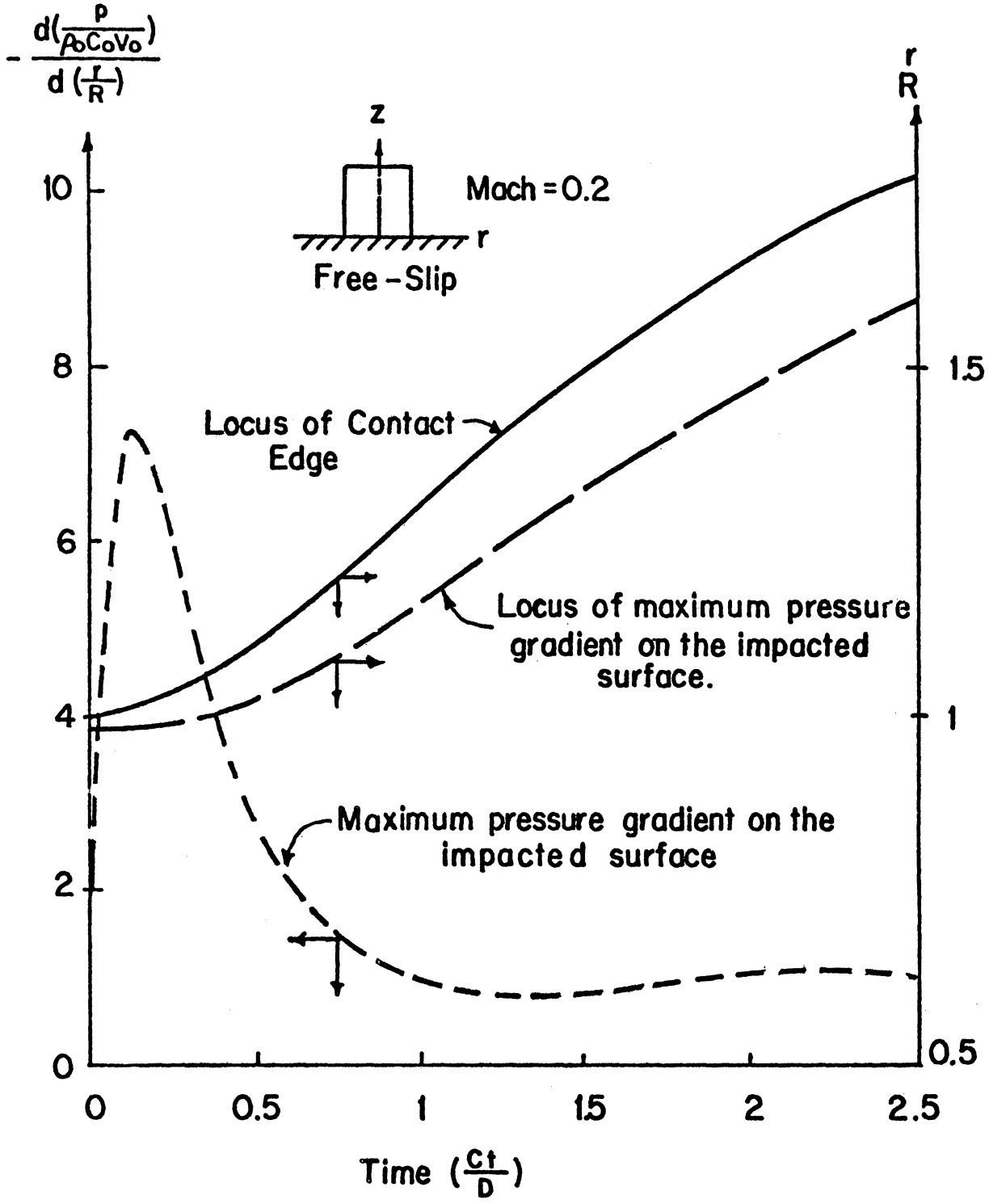

Fig. 7. Maximum Pressure Gradient-Time and -Location Relation and Contact Edge-Time History of an Initially Cylindrical Droplet with L/D = 1, for Impact Mach Number of 0.2 and for Free-Slip Boundary Condition.

V. REFERENCES

Batchelor, G.K. 1967 An Introduction to Fluid Dynamics. Cambridge University Press.

Briggs, L.J. 1950 Limiting negative pressure of water. J. Appl. Phys. 21, 721-722.

Bowden, F.P. & Brunton, J.H. The deformation of solids by liquid impact at supersonic speeds. Proc. Roy. Soc. A 263, 433-450.

Burstein, S.Z. 1967 Finite-difference calculations for hydrodynamic flows containing discontinuities. J. Comput. Phys. 2, 198-222.

Cole, R.H. 1965 Underwater Explosions. Dover.

Heymann, F.J. 1968 On the shock wave velocity and impact pressure in high-speed liquid-solid impact. J. Basic Engng. Trans. ASME 90, 400-402.

Huang, Y.C. 1971 Ph.D. Thesis, University of Michigan.

Lax, P. & Wendroff, B. 1960 System of conservation laws. Communication on Pure and Appl. Math. 13, 217-237.

Richtmyer, R.D. & Morton, K.W. 1967 Difference Methods for Initial Value Problems. Inter-Science.

Rubin, E.L. 1967 Difference methods for the inviscid and viscous equations of a compressible gas. J. Comput. Phys. 2, 178-196.

Schlichting, H. 1960 Boundary Layer Theory. McGraw-Hill.

Tait, P.G. 1888 Report on some of the physical properties of fresh water and sea water. Phys. Chem. 2, 1-71.